Environmental Science and Pollution Research (2023) 30:71574–71584
https://doi.org/10.1007/s11356-021-13627-w

CIRCULAR ECONOMY FOR GLOBAL WATER SECURITY

Fabrication of different SnO_2 nanorods for enhanced photocatalytic degradation and antibacterial activity

Govindhan Gnanamoorthy[1] · Virendra Kumar Yadav[2] · Krishna Kumar Yadav[3] · Kandasamy Ramar[4] · Javed Alam[5] · Arun Kumar Shukla[5] · Fekri Abdulraqeb Ahmed Ali[6] · Mansour Alhoshan[5,6]

Received: 17 January 2021 / Accepted: 21 March 2021 / Published online: 10 April 2021

Abstract

The acid-mediated (oxalic acid [OXA], cinnamic acid [CA], and itaconic acid [IA]) SnO_2 nanorods were synthesized by the hydrothermal method. The synthesized SnO_2 nanorods, in turn, were analyzed with various physico-chemical techniques such as the X-ray diffraction (XRD), Fourier transform infrared spectroscopy (FT-IR), scanning electron microscope (SEM), and Raman spectroscopy. Furthermore, the photocatalytic activity of the different SnO_2 nanorods was investigated with the malachite green (MG) dye under visible light illumination. The OXA-SnO_2 nanorods displayed an excellent degradation performance with observed value at 91% and it was compared to CA and IA-SnO_2 nanomaterials. This tetragonal phase was identified and confirmed by XRD studies. In this regards, obtained band gap energy is low then optimally performed to the photocatalytic evolution. The OXA-SnO_2 materials were tested for antibacterial and antifungal studies; this was as shown in good biological activities with admire to the different bacterial strains. The *Candida albicans* (antifungal) and *Enterococcus faecalis* (Gram-positive) bacteria were not affected in the microbial studies.

Keywords SnO_2 · Hydrothermal method · Acid-mediated · Malachite green dye · Photocatalyst · sAntibacterial

Introduction

A novel nanomaterial has most attractive and considered due to the photocatalytic applications. Recently, food and pharmaceuticals, textile, leather, and paper industries reported that materials containing several organic aromatic groups and molecules produced toxic gas and other moieties, which are highly damaging in an environment (Bouras and Slaoui 2019; Yadav et al. 2017). However, these dyes are highly toxic and affect human, animal, and bird health disorders and damaging ecosystems (Gruzeł 2019; Prasad et al. 2021; Gupta et al. 2021). Nowadays, pollution can be controlled with soluble dyes used in various fields in the emerging world. For instance, Sirajul (2019) reported that the Cd ions incorporated into the SnO_2 nanoparticles are favored for the absorption process and thermodynamic studies. Meanwhile, the researchers developed SnO_2-based nanomaterials for several applications such as in electrochemical sensors (Dilip and Jayaprakash 2018), solar cells (Liu et al. 2019), battery studies (Mao and Tian 2019), fuel cells (Dou et al. 2013), supercapacitors (Saravanakumar et al. 2019), biological studies (Srivastav et al. 2018; Singh et al. 2019; Sharma et al. 2015), and photocatalytic activities (Honarmand 2019). In

Responsible Editor: Philipp Gariguess

✉ Krishna Kumar Yadav
envirokrishna@gmail.com

✉ Javed Alam
javaalam@ksu.edu.sa

1 Department of Inorganic Chemistry, University of Madras, Guindy Campus, Chennai 600025, India

2 School of Life Sciences, Jaipur National University, Jaipur 302017, India

3 Faculty of Science and Technology, Madhyanchal Professional University, Ratibad, Bhopal 462044, India

4 PG & Research Department of Chemistry, Jamal Mohamed College, Trichy 20, India

5 King Abdullah Institute for Nanotechnology, King Saud University, P.O. Box 2455, Riyadh 11451, Saudi Arabia

6 Chemical Engineering Department, College of Engineering, King Saud University, P.O. Box 2455, Riyadh 11451, Saudi Arabia

case some people used different toxic chemicals and synthesis methods, it has been explained by the morphology and band gap energy. Therefore, the photocatalytic activity of different acid-mediated SnO_2 nanorods was tested.

Moreover, several metal oxides are currently reported to be used in the field of photocatalysis, such as ZnS-based materials (Tie et al. 2019), Sn(IV)/TiO_2/AC (Sun et al. 2006), Ag/ZnO (Hosseini et al. 2019; Zhang et al. 2017), PVDF/TiO_2 nanofibers (Dong et al. 2017), 3D g-C_3N_4 (Heo and Shukla 2019), and β-Bi_2O_3@Bi_2S_3 (Yu et al. 2018). However, these types of materials, created for the first time, displayed a better efficiency in photocatalytic performances with a well-known photo-generated recombination used in different light sources with respect to the various organic pollutants and dyes. These semiconductor materials possess more favorable photocatalytic studies boosting the degradation efficiency as well as exhibiting the synergistic effects.

This study aims to introduce the SnO_2 nanorods which have a tetragonal crystal system with the materials having been characterized by the surface morphology and various physico-chemical methods. The SnO_2 nanorod has a few advantages including being facile, eco-friendly, easily available, having mild reactions and reduced toxicity, and lower costs of the synthesized materials. The synthesized OXA, CA, and IA-SnO_2 nanomaterials were used for the photocatalytic studies under the visible light source with the malachite green dye. However, the OXA-SnO_2 nanomaterials gained a higher efficiency when compared with the CA and IA-SnO_2 nanomaterials.

Materials and methods

Materials

The number of standard chemicals required for the material synthesis was the recommended analytical grade chemicals, such as stannous chloride ($SnCl_2·2H_2O$), oxalic acid ($C_2H_2O_4$), cinnamic acid ($C_9H_8O_2$), and itaconic acid ($C_5H_6O_4$), with NaOH materials with methanol and ethanol used as solvents.

Synthesis of SnO_2 nanorods (OXA, CA, and IA-SnO_2)

The SnO_2 nanorods were first synthesized by the hydrothermal method. In a typical procedure, 1 mm of the $SnCl_2·2H_2O$ was dissolved in methanol, making three sets with each set of the solution added drop wise in different acids such as oxalic acid, cinnamic acid, and itaconic acid. These precursors were stirring for 1 h, then, the liquid NaOH (0.1M) was added and the solution stirred overnight for 12 h. The obtained homogeneous solution was then transferred to the stainless steel autoclave, maintaining the temperature at 180 °C. The obtained product was washed with ethanol and water several times, followed by drying at a vacuum oven at 25 °C overnight.

Antibacterial studies

The antibacterial activity of the SnO_2 nanorods was evaluated for the different pathogens by using the agar well diffusion method (Gnanamoorthy et al. 2020). This bacterial analysis was performed by the antibiotic condition. The synthesized SnO_2 nanorod was tested to the *Staphylococcus aureus* (Gram-positive), *Escherichia coli* (Gram-negative), *Pseudomonas aeruginosa* (Gram-negative), *Candida albicans* (antifungal), and *Enterococcus faecalis* bacteria (Gram-positive) all cultured from the Mueller-Hinton agar with incubated temperatures at 32–35 °C for 48 h. The 0.9% saline solution was used for washing with observed bacterial strain intensity OD values for 0.5 at 571 nm, and then different higher concentrations (100 μg/mL, 200 μg/mL, and 500 μg/mL) were added in the well and different positive controls (20 μg/mL) (*S. aureus*, *E. faecalis*—amoxicillin, *E. coli*, *P. aeruginosa*—levofloxacin, *C. albicans*—fluconazole) were used, after being measured for the zone of inhibition.

Characterization

The three different synthesized SnO_2 nanomaterials were characterized and confirmed by XRD (Rigaku, Dmax-2500) with the surface morphology images captured by SEM (Hitachi, S-4800). The phase orientation confirmation was recorded by FT-IR and Raman spectroscopy (WQF-410 and LABRAM-HR system with laser excitation of 514.5 nm). The dye degradation studies were carried out by UV-visible spectroscopy (Hitachi U-3010). The photocatalytic measurement was recorded by the photocatalytic reactor (Techinstro).

Results and discussion

Structural analysis

The three different SnO_2 nanorods were synthesized by the hydrothermal method. Figure 1a–c shows the XRD patterns of the synthesized materials and observed all the diffraction Bragg peak positions compared to the reference and well-matched with JCPDS card no. 10-1854. The sharp peaks seem to assemble SnO_2 nanorods with different acids' sample methods. The obtained diffraction peaks at 26.0°, 33.9°, 38.1°, 51.8°, 54.2°, 57.9°, 61.9°, 64.7°, 65.9°, 71.3°, and 78.6° corresponding to the (110), (101), (200), (211), (220), (002), (120), (112), (301), (250), and (321) planes. The synthesized SnO_2 nanorods were identified the tetragonal system in all three samples. The CA and IA-SnO_2 samples obtained

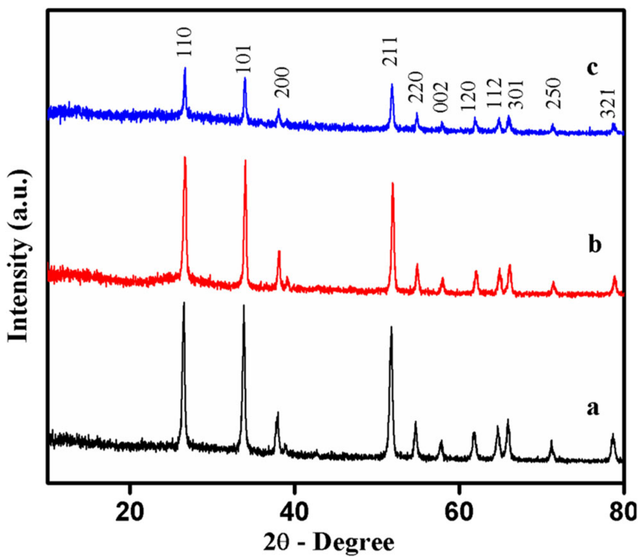

Fig. 1 XRD patterns of **a** OXA, **b** CA, and **c** IA-SnO_2 nanorods

for the lower intensity had some differences when compared to the OXA-SnO_2 nanorods. These three acid-mediated SnO_2 nanorods showed diffraction peaks without shifting 2θ values than the lattice parameter which also increased. The OXA, CA, and IA-SnO_2 nanorod crystallite sizes were calculated by the Debye-Scherrer formula (Eq. 1).

$$HO_2^{-\bullet}H_2O \rightarrow H_2O_2 + OH \quad (1)$$

Here, K is the shape factor, the wavelength, and the diffraction angle. The evaluated crystallite size is in decreasing order of the materials, OXA-SnO_2 > CA-SnO_2 > IA-SnO_2 nanomaterials, 38 nm, 37 nm, and 32 nm, respectively.

FT-IR spectroscopy

The chemical composition of the three different synthesized SnO_2 nanorods was characterized by the FT-IR spectroscopy method. The SnO_2 nanorods' FT-IR comparison spectra are shown in Fig. 2a–c and evaluated by the several vibration peaks. The vibration peak at 400–640 cm^{-1} corresponds to the O-Sn-O and Sn-O stretching vibrations which is similar to the previously reported work (Chen et al. 2015; Yadav et al. 2021). The peak 1608 cm^{-1} is attributed to the bending vibration modes of the N-H group and 3340 cm^{-1} can be ascribed to the O-H stretching or N-H stretching vibrations of absorbed water molecules (Gnanamoorthy et al. 2019; Tavker et al. 2021). The CA-SnO_2 nanoparticles' vibration peak transmittance has been decreased depending on the formation of molecules. Hence, synthesized SnO_2 functional groups were confirmed and the results coincide with the Raman spectroscopy. Therefore, the materials' functional groups were confirmed, which have been used for the subsequent application process.

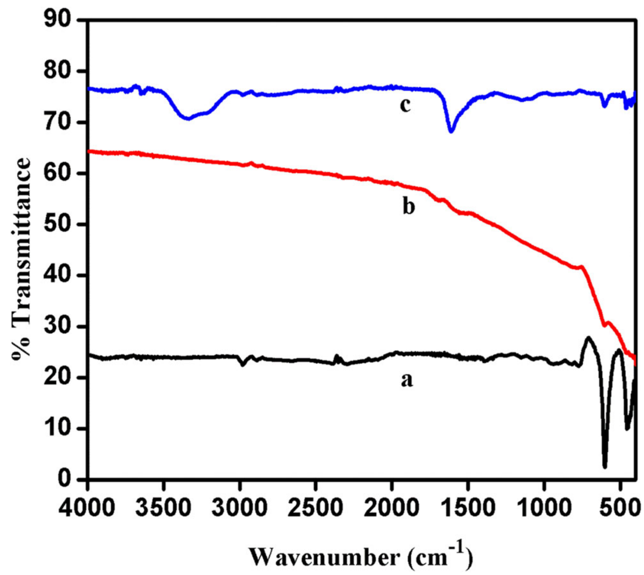

Fig. 2 FT-IR spectra of **a** OXA, **b** CA, and **c** IA-SnO_2 nanorods

Raman spectroscopy

Figure 3a–c shows the Raman spectra of the OXA, CA, and IA-SnO_2 nanorods, the three peaks appeared with good agreement results. The overall characteristic peaks are at 240, 472, and 627 cm^{-1} which are associated with the A_1g vibration mode at 625 cm^{-1}. The peaks 240 and 472 cm^{-1} are the Eg vibration modes of different SnO_2 nanorods (Hui Liu et al. 2019). The other peak at 240 cm^{-1} is the companion peak associated with the vibration $\upsilon 1^c(A_1^c)$ of the edge-sharing of the SnO_2 structure.

DRS UV-visible spectroscopy

The OXA, CA, and IA-SnO_2 nanorods' diffuse reflectance spectroscopy results were shown in Fig. 4a–c. The SnO_2

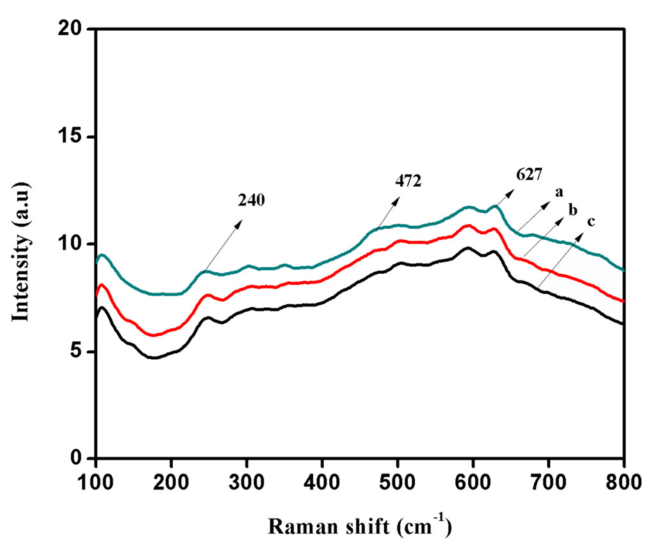

Fig. 3 Raman spectra of **a** OXA, **b** CA, and **c** IA-SnO_2 nanorods

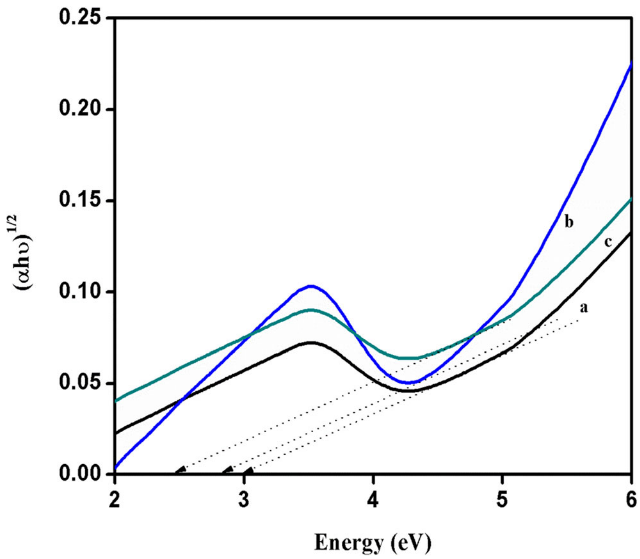

Fig. 4 Band gap energy of acid-mediated **a** IA, **b** CA, and **c** OXA-SnO_2 nanorods

nanorods were synthesized at a temperature of 180 °C and the optical band gap energy was evaluated using the Kubelka-Munk equation (given below Eq. 2).

$$\alpha hv = A(\text{hv}-\text{Eg}) \quad (2)$$

where α is the proportionality constant, A the absorption coefficient, hν the Planck constant, and Eg the band gap respectively. The obtained DRS-UV results show that the OXA, CA, and IA-SnO_2 nanorods have identified red shift regions of the transition. The OXA, CA, and IA-SnO_2 nanoparticles' band gap energies (in-direct) were at 2.5 eV, 2.8 eV, and 3.0 eV, while preparing the low band gap energy compared to the reported band gap values (Yadav et al. 2020a; Kar et al. 2019). The OXA-SnO_2 nanoparticles exhibited lower band gap energies (in-direct) when compared to the CA and IA-SnO_2 materials. As a result, all these SnO_2 nanomaterials were used to enhance the photocatalytic performances.

Morphology studies

Figure 5a–d shows the scanning electron microscope images of OXA-SnO_2 and these images explained by the nanorod like structure with bundles of rods edge-to-edge carefully merging with each other and obtained with a diameter range of 3–1 µm. The CA-SnO_2 surface morphology is shown in Fig. 6a–d, the synthesized material has shown layers like structure with diameter ranges 1, 2, and 10 µm. The IA-SnO_2 surface morphology is shown in Fig. 7a–d and the morphology illustrated that the tube tablet-like structure with a diameter range of 300 to 500 nm. All the synthesized SnO_2 nanomaterials were confirmed by various techniques and have shown low band gap energy, therefore, the photocatalytic activity should be enhanced.

Fig. 5 **a**–**d** SEM images of OXA-SnO_2 nanorods

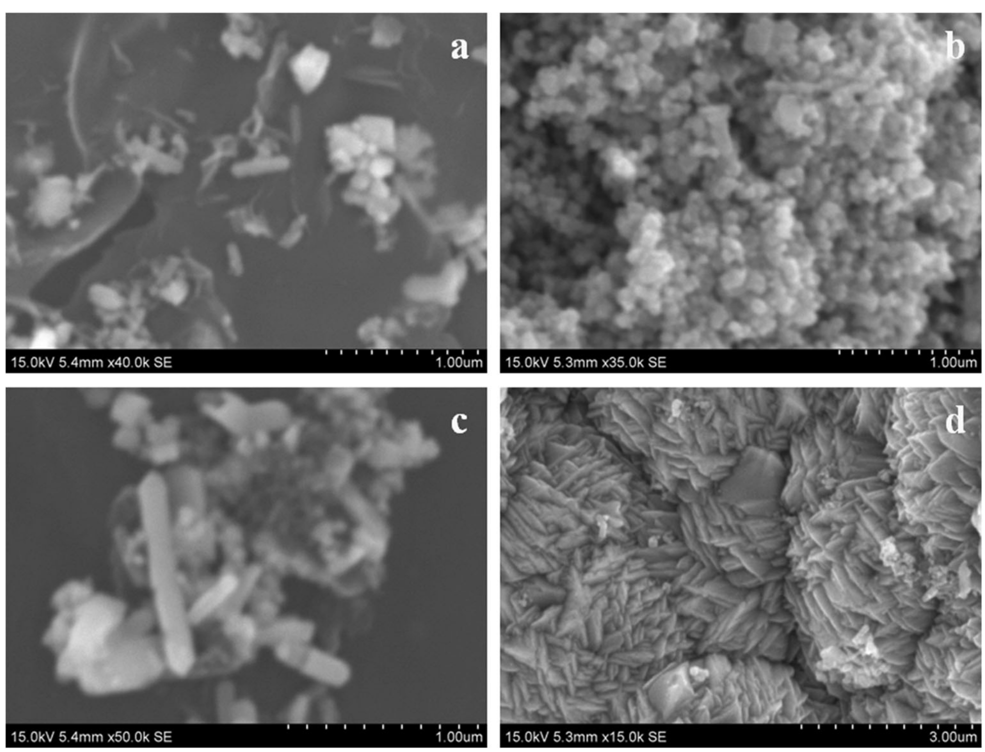

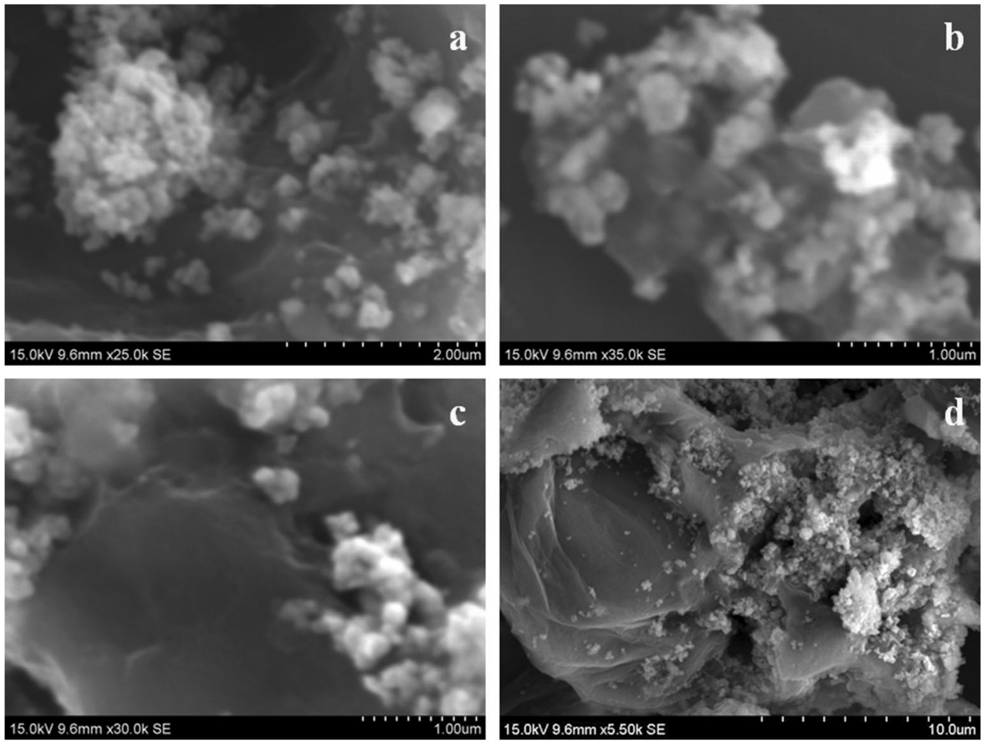

Fig. 6 **a**–**d** SEM images of CA-SnO_2 nanorods

Photocatalytic activity

Figures 8a–d, 9a–d, and 10a–d explain that the absorption spectra of the MG photodegradation in the presence of different SnO_2 nanorods showed a maximum absorption range at 630 nm. Figures 8a, 9a, and 10a show the evidence of the photocatalyst dye degradations of the MG under visible light illumination of 500 nm. Figures 8b, 9b, and 10b display the function of time (Ct/C_0) and the photodegradation with respect to concentration and the reaction time. Figures 8c, 9c,

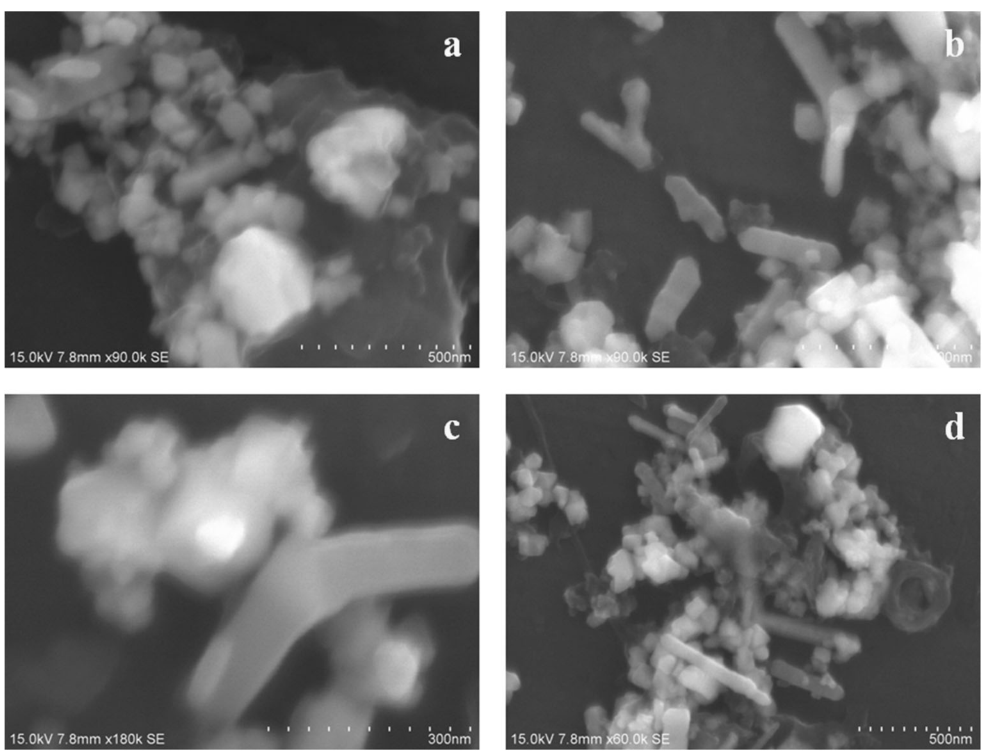

Fig. 7 **a**–**d** SEM images of IA-SnO_2 nanorods

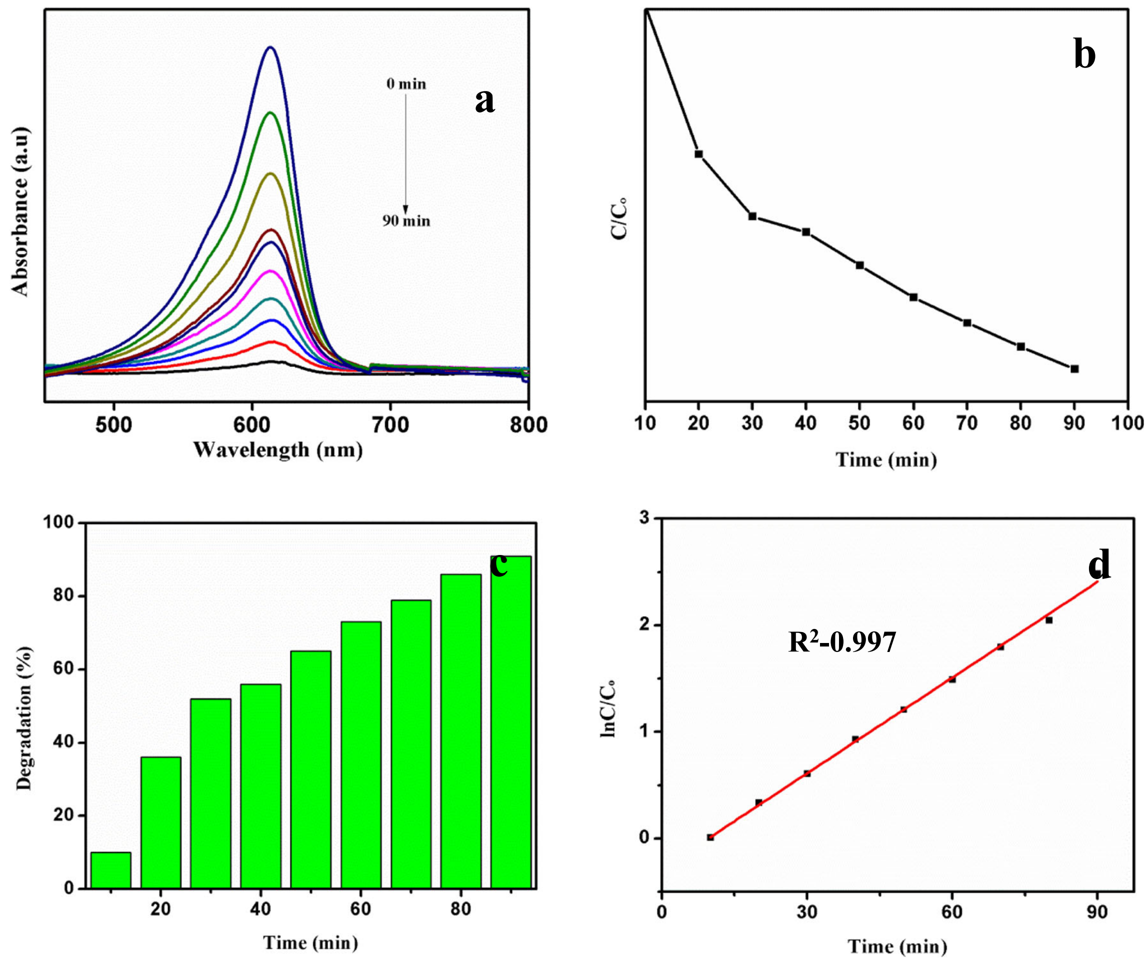

Fig. 8 **a** Dye degradation, **b** concentration of C/C_o, **c** percentage of degradation, and **d** rate constant of OXA-SnO_2 nanorods

and 10c illustrate the calculated degradation percentage, here the OXA-SnO_2 nanorods have been shown an excellent degradation compared to other mediated SnO_2 nanomaterials, the kinetic first order scan rate was calculated and the value found to be $R^2 = 0.997$, 0.997, and 0.988 and the slope value 0.0299, 0.0184, and 0.034 for OXA-SnO_2, CA-SnO_2, and IA-SnO_2, respectively. However, the intensity of the adsorption peak decreased within 90, 60, and 50 min, the monitored degradation (Figs. 8d, 9d, and 10d) process percentages at 91, 78, and 66. Summarized, the synthesized different SnO_2 nanorods evaluated an excellent photocatalytic performance under the visible light source.

The obtained degradation efficiency of the SnO_2 nanomaterials such as OXA-SnO_2 and CA-SnO_2 nanoparticles are 78% and 66%, the results of which show low degradation efficiency with electron transfer when compared to the OXA-SnO_2 due to it having low bandgap energy. This band gap energy plays a key role in the formation of desirable defects of suitable photocatalytic behavior. In the presence of visible light, the acid-mediated SnO_2 nanomaterials produced charge recombination barriers in the valance and conduction bands. For the conduction band, the whole pair of H_2O/OH^- interacted with the hydroxyl ($OH^·$) in a radical formation, the conduction band of O_2 produced to the $O_2^{·-}$ and $HO_2^·$ were converted to H_2O_2 and $OH^·$ formation which strongly separates the radical formation with equation is shown below and detailed mechanism has been displayed in Fig. 11.

$$\text{OXA}-\text{SnO}_2 + \text{Visible light} \rightarrow \text{OXA}-\text{SnO}_2(\text{h}^+ + \text{e}^-) \quad (3)$$

$$\text{O}_2 + \text{e}^- \rightarrow \text{O}_2^- \quad (4)$$

$$\text{H}_2\text{O} \rightarrow \text{h}^+ \rightarrow + \text{OH}^\bullet + \text{H}^+ \quad (5)$$

$$\text{O}_2^{-\bullet} + \text{H}^+ \rightarrow \text{HO}_2 \quad (6)$$

$$\text{HO}_2^{-\bullet} + \text{H}_2\text{O} \rightarrow \text{H}_2\text{O}_2 + \text{OH} \quad (7)$$

$$\text{OH}^\bullet + \text{Malachite Green} \rightarrow \text{Degradation products}$$

Therefore, the above experimental results suggest that the synthesized SnO_2 nanomaterial was enhanced to the photocatalytic dye degradation and the OXA-SnO_2 nanorods have enhanced the photocatalytic activity when compared to other reported materials (Kaviyarasu et al. 2016, Shelja Sharma

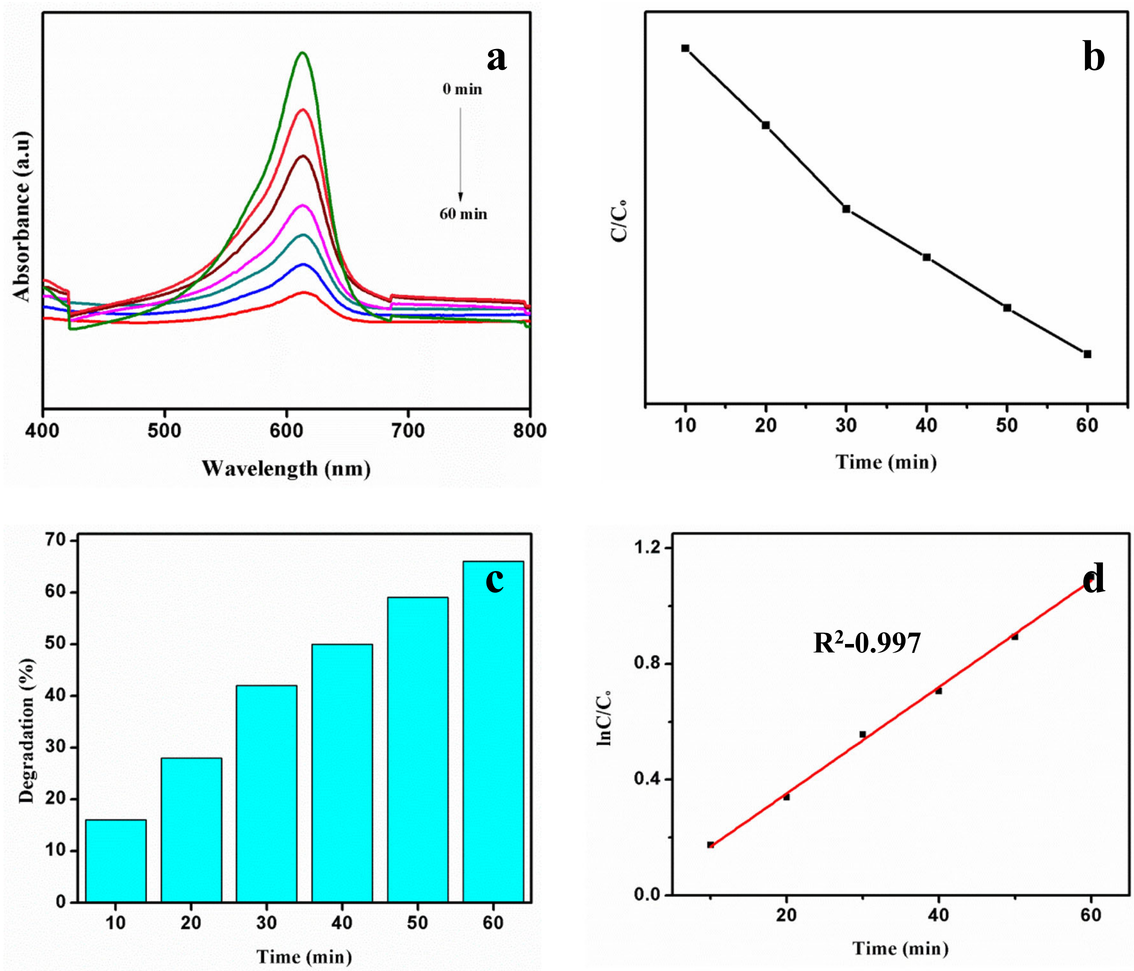

Fig. 9 **a** Dye degradation, **b** concentration of C/C_o, **c** percentage of degradation, and **d** rate constant of CA-SnO_2 nanorods

et al. 2020 and Meenu Meenu et al. 2020). This SnO_2 material was repeated for four times recycled and did not varying to degrading curves, which were shown in Fig. 12.

Antibacterial and antifungal activities

SnO_2 nanoparticles were analyzed for antibacterial and antifungal activities, which corresponds to the *Staphylococcus aureus* (Gram-positive), *Escherichia coli* (Gram-negative), *Pseudomonas aeruginosa* (Gram-negative), *Candida albicans* (antifungal), and *Enterococcus faecalis* bacteria (Gram-positive) zones of inhibition shown in Fig. 13a–e. Here, the first three bacteria (*Staphylococcus aureus* (Gram-positive), *Escherichia coli* (Gram-negative), *Pseudomonas aeruginosa* (Gram-negative)) have higher antibacterial activity due to the particle size and Sn^{2+} ions (Al-Hada et al. 2018; Yadav et al. 2020b). The *Candida albicans* (antifungal) and *Enterococcus faecalis* bacteria (Gram-positive) are not inhibited by the activity (Table 1). Among them, the strains were tested only for higher concentrations, as the lower concentration did not support the activity. Therefore, this SnO_2 material shown higher inhibition as compared to the results reported by Phukan et al. (2017) and Arularasu et al. (2018).

Conclusion

All three different (OXA, IA, and CA-SnO_2) nanorods were synthesized by the hydrothermal method. The prepared nanomaterial structure, functional groups, and the surface morphology were investigated and confirmed by the XRD, FT-IR, SEM, and Raman analysis. The XRD results confirmed the tetragonal structure of the SnO_2 nanorods and the metal oxide functional groups were identified and confirmsed by the FT-IR analysis. The peak at 240 to 700 cm^{-1} is different modes of M-O and M-O-M orientation and these results were similar to the FT-IR spectroscopy. This synthesized material has well-known specifications like low cost, easily available, eco-friendly, reusable, etc., then we are encourage and designed for this new material. OXA, IA, and CA-SnO_2 nanorods were applied to the photocatalytic performances with commonly used for malachite green dye. The synthesized

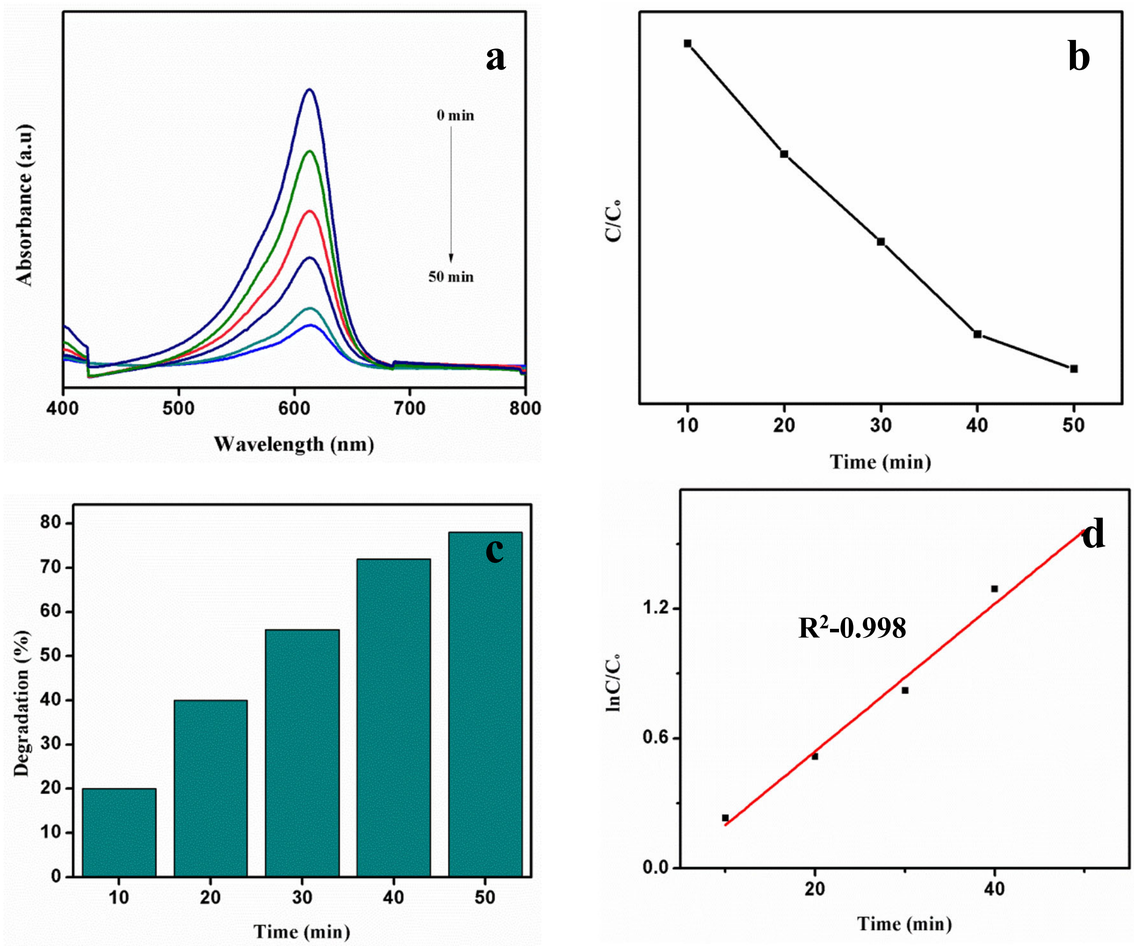

Fig. 10 **a** Dye degradation, **b** concentration of C/C_o, **c** percentage of degradation, and **d** rate constant of IA-SnO_2 nanorods

SnO_2 nanomaterials enhanced the degradation; meanwhile, the OXA-SnO_2 nanorods displayed an excellent photocatalytic performance when compared to the other synthesized IA and CA-SnO_2 materials. The OXA-SnO_2 materials have a superior stability nature. We are expecting in this materials may be used in future with an energy and biological applications. OXA-SnO_2 nanomaterial was testing for the antimicrobial studies like different pathogens, in this case *Staphylococcus aureus* (Gram-positive), *Escherichia coli* (Gram-negative), and *Pseudomonas aeruginosa* (Gram-negative) bacteria have performed with

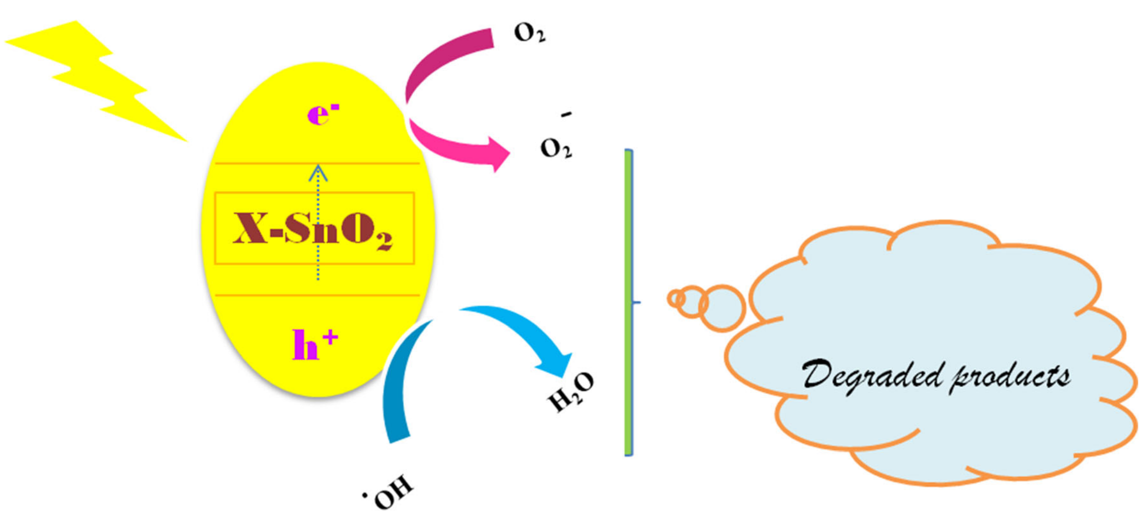

Fig. 11 Degradation mechanism of X-SnO_2 nanomaterials

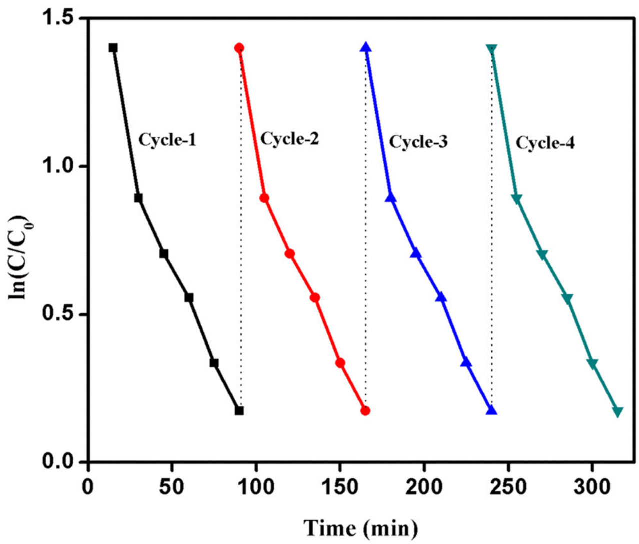

Fig. 12 Stability effect of SnO_2 nanorods

effectively and *Candida albicans* (antifungal) and *Enterococcus faecalis* bacteria (Gram-positive) pathogens are not supporting in antibacterial activity. These all result was satisfactory to the biological applications in future.

Acknowledgements The authors are indebted to the Department of Inorganic Chemistry, University of Madras, Guindy Campus, Chennai, for all the valuable support and needful facilities.

Author contribution GG and VKY investigated the samples XRD, FTIR, Raman spectroscopy, DRS UV-Vis spectroscopy, and SEM. KKY, KR, and JA interpreted their results. AK, FAAA, and MA critically reviewed the manuscript. All authors equally contributed to prepare the original draft of the manuscript.

Funding The authors extend their appreciation to the Deputyship for Research & Innovation, "Ministry of Education" in Saudi Arabia for funding this research work through the project number IFKSURG-1439-085.

Table 1 Antibacterial activity against different pathogens with positive controls of amoxicillin, levofloxacin, and fluconazole

S. no.	Pathogens	1 mg/mL	2 mg/mL	5 mg/mL	Positive control	Negative control
1	*S. aureus*	28	30	32	32	–
2	*E. coli*	28	28	30	34	–
3	*P. aeruginosa*	25	27	32	38	–
4	*C. albicans*	–	–	–	–	–
5	*E. faecalis*	–	–	–	–	–

Zone of inhibition: concentration (20 μg/mL) used for different positive control

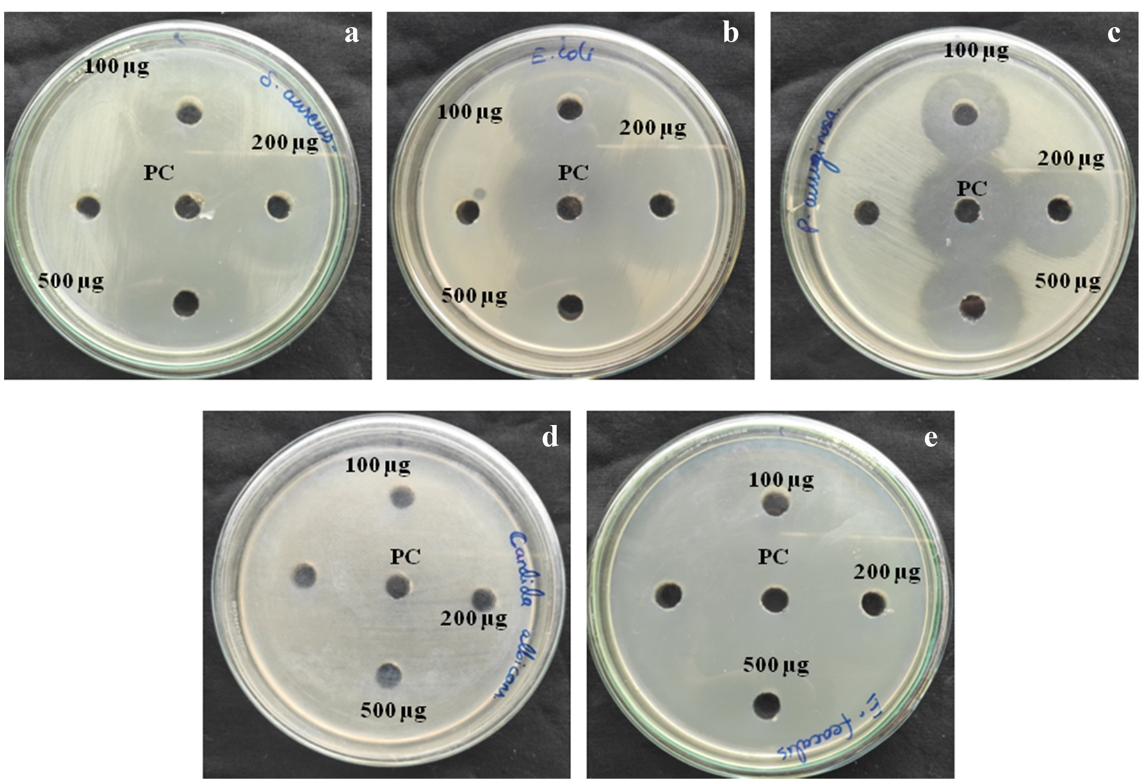

Fig. 13 SnO_2 nanoparticles antibacterial and antifungal studies: **a** *S. aureus* (Gram-positive), **b** *E. coli* (Gram negative), **c** *P. aeruginosa* (Gram-negative), **d** *C. albicans* (antifungal), and **e** *E. faecalis* bacteria (Gram-positive)

Data Availability Data sharing not applicable to this article as no datasets were generated or analyzed during the current study.

Declarations

Ethics approval

Not applicable.

Consent to participate Not applicable.

Consent for publication

Not applicable.

Competing interests The authors declare no competing interests.

References

Al-Hada NM, Kamari HM, Baqer AA, Shaari AH, Saion E (2018) Thermal calcination-based production of SnO_2 nanopowder: an analysis of SnO_2 nanoparticle characteristics and antibacterial activities. Nanomater 8:250. https://doi.org/10.3390/nano8040250

Arularasu MV, Anbarasu M, Poovaragan S, Sundaram R, Kanimozhi K, Magdalane MC, Kaviyarasu K, Thema FT, Letsholathebe D, Mola GT, Maaza M (2018) Structural, optical, morphological and microbial studies on SnO_2 nanoparticles prepared by Co-precipitation method. J Nanosci Nanotechnol 18:3511–3517. https://doi.org/10.1166/jnn.2018.14658

Bouras K, Slaoui A (2019) Photon management properties of Yb-doped SnO_2 nanoparticles synthesized by sol-gel technique. Phys Chem Chem Phys 1-24. https://doi.org/10.1039/C9CP01993F.

Chen H, Ding L, Sun W, Jiang Q, Hu J, Li J (2015) Synthesis and characterization of Ni doped SnO_2 microspheres with enhanced visible-light photocatalytic activity. RSC Adv 5:56401–56409. https://doi.org/10.1039/C5RA10268E

Dilip R, Jayaprakash R (2018) Synthesis and characterization of $BaFe_2O_4$ nano-ferrites for gas sensor applications. Energy, Ecology Environ 3:237–241. https://doi.org/10.1007/s40974-018-0093-z

Dong C, Fu Y, Zang W, He H, Xing L, Xue X (2017) Self-powering/self-cleaning electronic-skin basing on PVDF/TiO_2 nanofibers for actively detecting body motion and degrading organic pollutants. Appl Surf Sci 416:424–431. https://doi.org/10.1016/j.apsusc.2017.04.188

Dou M, Hou M, Liang D, Lu W, Shao Z, Yi B (2013) SnO_2 nanocluster supported Pt catalyst with high stability for proton exchange membrane fuel cells. Electrochim Acta 92:468–473. https://doi.org/10.1016/j.electacta.2013.01.070

Gnanamoorthy G, Yadav VK, Latha D, Karthikeyan V, Narayanan V (2019) Enhanced photocatalytic performance of $ZnSnO_3$/rGO nanocomposite. Chem Phys Lett 739:137050. https://doi.org/10.1016/j.cplett.2019.137050

Gnanamoorthy G, Yadav VK, Narayanan V (2020) Well organized assembly of (X)-$CuSnO_3$ nanoparticles enhanced photocatalytic and anti-bacterial properties. J Water Process Eng 36:101258. https://doi.org/10.1016/j.jwpe.2020.101258

Gruzeł G (2019) Preparation of Pt-skin PtRhNi nanoframes decorated with small SnO_2 nanoparticles as an efficient catalyst for ethanol oxidation reaction. ACS Appl Mater Interfaces 11:22352–22363. https://doi.org/10.1021/acsami.9b04690

Gupta N, Yadav KK, Kumar V, Krishnan S, Kumar S, Nejad ZD, Khan MAM, Alam J (2021) Evaluating heavy metals contamination in soil and vegetables in the region of North India: levels, transfer and potential human health risk analysis. Environ Toxicol Pharmacol 82:103563. https://doi.org/10.1016/j.etap.2020.103563

Heo NS, Shukla S (2019) Shape-controlled assemblies of graphitic carbon nitride polymer for efficient sterilization therapies of water microbial contamination via 2D g-C_3N_4 under visible light illumination, Mater. Sci Eng C 104:109846. https://doi.org/10.1016/j.msec.2019.109846

Honarmand M (2019) Biosynthesis of tin oxide (SnO_2) nanoparticles using jujube fruit for photocatalytic degradation of organic dyes. Adv Powder Technol 30:1551–1557. https://doi.org/10.1016/j.apt.2019.04.033

Hosseini M, Fazelian N, Fakhri A, Kamyab H, Yadav KK, Chelliapan S (2019) Preparation, and structural of new NiS-SiO_2 and Cr_2S_3-TiO_2 nano-catalyst: photocatalytic and antimicrobial studies. J Photochem Photobiol B Biol 194:128–134. https://doi.org/10.1016/J.JPHOTOBIOL.2019.03.016

Kar A, Olszowka J, Sain S et al (2019) Morphological effects on the photocatalytic properties of SnO_2 nanostructures. J Alloys Compd 810:151718. https://doi.org/10.1016/j.jallcom.2019.151718

Kaviyarasu K, Kennedy J, Manikandan E, Henini M, Malik M (2016) Photodegradation of organic pollutants RhB dye using UV simulated sunlight on ceria based TiO_2 nanomaterials for antibacterial applications. Sci Rep 6:38064. https://doi.org/10.1038/srep38064

Liu D, Wang Y, Xu H, Zheng H, Zhang T, Zhang P, Wang F, Wu J, Wang Z, Chen Z, Li S (2019) SnO_2-based perovskite solar cells: configuration design and performance improvement. Sol RRL 3:1800292. https://doi.org/10.1002/solr.201800292

Mao Y, Tian Q (2019) Improving the lithium storage performance of SnO_2 nanoparticles by in-situ embedding into a porous carbon framework. J Alloys Compd 803:224–230. https://doi.org/10.1016/j.jallcom.2019.06.251

Meenu S, Dehiya BS, Umar A (2020) VO_2(M)@CeO_2 core-shell nanospheres for thermochromic smart windows and photocatalytic applications. Ceram Int 46:986–995. https://doi.org/10.1016/j.ceramint.2019.09.062

Phukan A, Bhattacharjee RP, Dutta DK (2017) Stabilization of SnO_2 nanoparticles into the nanopores of modified montmorillonite and their antibacterial activity. Adv Powder Technol 28:139–145. https://doi.org/10.1016/j.apt.2016.09.005

Prasad S, Yadav KK, Kumar S, Gupta N, Cabral-Pinto MMS, Rezania S, Radwan N, Alam J (2021) Chromium contamination and effect on environmental health and its remediation: a sustainable approaches. J Environ Manag 285:112174. https://doi.org/10.1016/j.jenvman.2021.112174

Saravanakumar B, Ravi G, Ganesh V (2019) Low surface energy and pH effect on SnO_2 nanoparticles formation for supercapacitor applications. J Nanosci Nanotechnol 19:3429–3436. https://doi.org/10.1166/jnn.2019.16098

Sharma S, Kumar V, Yadav KK, Gupta N, Verma C (2015) Long-term assessment of fly ash disposal on physico-chemical properties of soil. Int J Curr Res Biosci Plant Biol 2:105–110

Sharma S, Ibhadon AO, Francesconi MG, Mehta SK, Elumalai S, Kansal SK, Umar A, Baskoutas S (2020) Bi_2WO_6/C-Dots/TiO_2: a novel Z-scheme photocatalyst for the degradation of fluoroquinolone levofloxacin from aqueous medium. Nanomaterials 10:910. https://doi.org/10.3390/nano10050910

Singh AV, Jahnke T, Xiao Y, Wang S, Wang S, Yu Y, David H, Richter G, Laux P, Luch A, Srivastava A, Saxena PS, Bill J, Sitti M (2019) Peptide-induced biomineralization of tin oxide (SnO_2) nanoparticles for antibacterial applications. J Nanosci Nanotechnol 19:5674–5686. https://doi.org/10.1166/jnn.2019.16645

Sirajul H (2019) Adsorption of Cd^{2+} ions onto SnO_2 nanoparticles synthesized via sol-gel method: physiochemical study. Mater Res Express 6:105035. https://doi.org/10.1088/2053-1591/ab38c8

Srivastav A, Yadav KK, Yadav S, Gupta N, Singh JK, Katiyar R, Kumar V (2018) Nano-phytoremediation of pollutants from contaminated soil environment: current scenario and future prospects. Springer, Cham, pp 383–401

Sun J, Wang X, Sun J, Sun R, Sun S, Qiao L (2006) Photocatalytic degradation and kinetics of orange G using nano-sized Sn(IV)/

TiO_2/AC photocatalyst. J Mol Catal A Chem 260:241–246. https://doi.org/10.1016/j.molcata.2006.07.033

Tavker N, Yadav VK, Yadav KK, Cabral-Pinto MMS, Alam J, Shukla AK, Fekri MA, Ali AA (2021) Removal of cadmium and chromium by mixture of silver nanoparticles and nano-fibrillated cellulose isolated from waste peels of Citrus sinensis. Polymer 13:234. https://doi.org/10.3390/polym13020234

Tie L, Sun R, Jiang H, Liu Y, Xia Y, Li Y, Chen H, Yu C, Dong S, Sun J, Sun J (2019) Facile fabrication of N-doped ZnS nanomaterials for efficient photocatalytic performance of organic pollutant removal and H_2 production. J Alloys Compd 807:151670. https://doi.org/10.1016/j.jallcom.2019.151670

Yadav KK, Singh JK, Gupta N, Kumar V (2017) A review of nanobioremediation technologies for environmental cleanup: a novel biological approach. J Mater Environ Sci 8:740–757

Yadav VK, Yadav KK, Gnanamoorthy G, Choudhary N, Khan SH, Kamyab H, Bach Q-V (2020a) Novel synthesis and characterization of polyhedral shaped amorphous iron oxide nanoparticles from incense sticks ash waste. Environ Technol Innov 20:101089. https://doi.org/10.1016/j.eti.2020.101089

Yadav VK, Ali D, Khan SH, Gnanamoorthy G, Choudhary N, Yadav KK, Thai VN, Hussain SA, Manhrdas S (2020b) Synthesis and characterization of amorphous iron oxide nanoparticles by the sonochemical method and their application for the remediation of heavy metals from wastewater. Nanomaterials 10:1551. https://doi.org/10.3390/nano10081551

Yadav VK, Gnanamoorthy G, Cabral-Pinto, MMS, Alam, J, Ahamed, M, Gupta N, Singh B, Choudhary, N, Inwati GK, Yadav KK (2021) Variations and similarities in structural, chemical and elemental properties on the ashes derived from the coal due to their combustion in open and controlled manner. Environ Sci Pollut Res. Accepted.

Yu C, Yang P, Tie L, Yang S, Dong S, Sun J, Sun J (2018) One-pot fabrication of β-Bi_2O_3@Bi_2S_3 hierarchical hollow spheres with advanced sunlight photocatalytic RhB oxidation and Cr(VI) reduction activities. Appl Surf Sci 455:8–17. https://doi.org/10.1016/j.apsusc.2018.04.201

Zhang L, Zhu D, He H, Wang Q, Xing L, Xue X (2017) Enhanced piezo/solar-photocatalytic activity of Ag/ZnO nanotetrapods arising from the coupling of surface plasmon resonance and piezophototronic effect. J Phys Chem Solids 102:27–33. https://doi.org/10.1016/j.jpcs.2016.11.009